Supporting Information

for

Characterizing the Opportunity Space for Sustainable Hydrothermal Valorization of Wet Organic Wastes

Jianan Feng[1], Yalin Li[2], Timothy J. Strathmann[3], Jeremy S. Guest[1,4,*]

[1] Department of Civil and Environmental Engineering, University of Illinois Urbana-Champaign, Urbana, Illinois 61801, United States

[2] Department of Civil and Environmental Engineering, Rutgers, The State University of New Jersey, Piscataway, New Jersey 08854, United States

[3] Department of Civil and Environmental Engineering, Colorado School of Mines, Golden, Colorado 80401, United States

[4] Institute for Sustainability, Energy, and Environment, University of Illinois Urbana-Champaign, Urbana, Illinois 61801, United States

* Jeremy S. Guest: email: jsguest@illinois.edu phone: (217) 244-9247

This Supporting Information contains 32 pages, 14 tables, and 7 figures.

S1. Feedstock characterization

Organic wastes serving as feedstocks for the HTL-based treatment train were characterized based on their moisture content, ash content, and biochemical compositions (lipids, proteins, carbohydrates) (**Table S1**). Based on these assumptions, their elemental compositions were also estimated based on a multi-component linear relationship (**Table S2**). Specifically, carbon, hydrogen, and nitrogen content of lipids ($C_8H_{16}O$), proteins ($C_{16}H_{24}O_5N_4$), and carbohydrates (CH_2O) were estimated based on their empirical chemical formula.[1] Phosphorus was estimated based on reported nitrogen to phosphorus ratio for different feedstocks (**Table S1**). Oxygen was estimated based on mass balance as 1 – C (dry weight, dw%) – H (dw%) – N (dw%) – P (dw%) – ash (dw%).

Table S1. Biochemical compositions of different organic wastes.

Organic Waste	Moisture [%]	Ash [dry weight%]	Biochemical compositions [ash-free dry weight%]			P to N mass ratio	Ref.
			Lipids	Proteins	Carbohydrates		
Sludge	60−80%	17.4−41.4%	8−30.8%	38−51%	100% – lipids% – proteins%	19.4−55.6%	[2–6]
Fats, oils, and greases (FOG)	10−60%	1.49−2.24%	91.2−100%	0−1.23%		0−3.5%	[7–10]
Food waste	68−80%	2.5−12.6%	13–30%	15−25%		11.5−28.6%	[5,6,10–12]
Green waste	5.2−69%	1.2−48.3%	1.04−2.59%	1.6−8.2%		18.7−22.9%	[13–15]
Animal manure	17.4−79.8%	13.8−43%	3.77−24.7%	14.3−26.4%		25.3−38.0%	[3,4,16]

Table S2. Coefficients used for the estimation of elemental compositions of organic wastes.

	Lipids ($C_8H_{16}O$)	**Proteins** ($C_{16}H_{24}O_5N_4$)	**Carbohydrates** (CH_2O)
C	0.750 (± 0.075)[a]	0.545 (± 0.055)[a]	0.400 (± 0.040)[a]
H	0.125 (± 0.013)[a]	0.068 (± 0.007)[a]	0.067 (± 0.007)[a]
N	–	0.159 (± 0.016)[a]	–

[a] Uniform distribution.

S2. System design

1. Design basis

The design for HTL-based treatment system was executed using newly released QSDsan[17,18] (using 'pfas' branch updated as of October 28, 2023), a comprehensive modeling platform for quantitative sustainable design of sanitation and resource recovery systems. All the units were coded using python 3.9 and can be publicly accessed through GitHub-Quantitative Sustainable Design (QSD) Group-repositories.[18] The proposed system configuration was based on a 2014 PNNL report,[19] with the addition of struvite precipitation and membrane distillation for nutrient recovery. Detailed unit design assumptions and methods can be found in the following sections. Units not discussed below (e.g., heat exchanger, flash vessel, distillation column) were inherited from previous work in QSDsan and BioSTEAM[20,21] (using 'qsdsan' branch updated as of October 28, 2023).

2. Detailed design assumptions and methods

i. Hydrothermal liquefaction (HTL)

HTL converted wet biomass into biocrude, hydrochar, an aqueous phase, and off-gas under subcritical temperatures (250 to 350 °C) and high pressure (3050 psia). We used a revised multi-component additivity (MCA) model[22,23] to estimate the yields and elemental compositions of each HTL product (**Table S3**). All calculations were done on an ash free dry weight (afdw) basis. Except for lipid-to-biocrude (0.846) which followed a triangular distribution, other parameters with uncertainties were assigned normal distributions. All ash content from HTL feedstocks were assumed to be partitioned into the aqueous phase (consistent with Leow et al.[23]). The gas phase was >90% CO_2 with a small amount of CH_4 and C_2H_6. The gas compositions were based on simulations from Jones et al.[19] Biocrude moisture content was 5.6%, the same as our reference model.[19]

Table S3. Revised MCA model parameters.

HTL Product	Lipids	Proteins	Carbohydrates
Biocrude	0.846 (0.692, 1.000)	0.445 (± 0.030)	0.205 (± 0.050)
Aqueous	0.154	0.481	–
Gas	–	0.074 (± 0.020)	0.418 (± 0.030)
Hydrochar	–	–	0.377

Elemental distributions in HTL oil and solid phases were calculated based on MCA model (**Table S4**), with AOSc (average oxidation state) calculated using the equation in Li et al.[22] Carbon in the gas phase was calculated based on estimated gas compositions. Nitrogen was assumed to partition to the biocrude and aqueous phases.[23,24] 86% (84 to 88%) of phosphorus was assumed to be in hydrochar after the HTL reaction in the form of inorganic phosphate.[24,25] The remaining phosphorus was assumed to be in the aqueous phase. The MCA model can also be used to estimate the TOC and TN concentrations (in $mg \cdot L^{-1}$) in the aqueous phase product, but in this study elements in the aqueous phase were calculated based on mass balance closure to accommodate uncertainties associated with the aqueous phase volume. The MCA was validated on wastewater sludge and animal manure in Li et al.[22] Validation for food waste, FOG, and green waste (limited to the biocrude yield) were included in **Table S5**. The auxiliary units for HTL include

knockout drums for gas separation, a solid filter for hydrochar recovery, and a gravimetric oil/water separator to vent gas and separate biocrude and aqueous phase by gravity, and knockout drums to remove any liquid from the off-gas.

Table S4. MCA model parameters for elemental composition of biocrude.

Elemental Composition	Input	Slope	Intercept
Biocrude-C	AOSc	–8.37 (± 1.84)	68.6 (± 0.72)
Biocrude-N	Protein [dw%]	0.133 (± 0.010)	–
Biocrude-H	AOSc	–2.61 (± 0.69)	8.20 (± 0.27)
Hydrochar-C[a]	Carbohydrate [dw%]	1.75 (± 0.24)	–

[a] The smaller value between the calculated result and 0.65 was used.

Table S5. Experimental data (from literature) and MCA predicted biocrude yields (for food waste, FOG, and green waste).

Waste	**Feedstock** [afdw%]			**Yield** [afdw%]		References
	Lipids	Proteins	Carbohydrates	Experimental	Predicted	
Food waste	16.6	29.1	54.3	28 to 30	32.0 to 44.3	[26]
Food waste	22.2	18.0	59.8	37.5	32.1 to 46.0	[27]
Food waste	~35	~24	~41	~40 to 46.9	40.5 to 56.9	[28]
Food waste	5.3	18.4	61.1	27.6	20.8 to 29.6	[9]
Food waste	19	27	54	45	32.7 to 45.6	[9]
Food waste	–	–	–	32 to 58	35.6 to 53.4	[29]
FOG	–	–	–	76.3	64.9 to 100	[30]
FOG	–	–	–	49 to 88	64.9 to 100	[9]
Green waste	0.7	10.8	80.4	23.3	17.4 to 26.3	[9]
Green waste	8	2	90	24.3	20.3 to 31.9	[9]
Green waste	–	–	–	4.4 to 40.9	16.5 to 29.2	[30,31]

As the feedstocks for HTL reactor at low temperatures have very high viscosity (0.002 to 0.065 $m^2 \cdot s^{-1}$),[32] the heat exchanger for HTL feedstock heating is typically overdesigned to overcome the potential fouling issue. In our design, we enforced the total heat transfer efficiency of HTL heat exchanger to 3 to 4 $BTU \cdot hr^{-1} \cdot ft^{-2} \cdot F^{-1}$ (0.0170 to 0.0227 $kW \cdot m^{-2} \cdot K$), which was an order of magnitude lower than the heat transfer efficiency of low-viscosity feedstock (26 to 274 $BTU \cdot hr^{-1} \cdot ft^{-2} \cdot F^{-1}$).[32] The HTL heat exchanger design process included the following steps:[21]

1. Calculated the log-mean temperature difference (*LMTD*) of an ideal counterflow or co-current heat exchanger using **Eq. S1** to **Eq. S5**.

$$dTF_1 = T_{h,I} - T_{c,o} \quad \text{(S1)}$$

$$dTF_2 = T_{h,o} - T_{c,i} \quad \text{(S2)}$$

$$dTF_{2,1} = dTF_2 - dTF_1 \quad \text{(S3)}$$

where $T_{h,I}$, $T_{c,o}$, $T_{h,o}$, and $T_{c,i}$ represented inlet temperature of hot fluid [K], outlet temperature of cold fluid [K], outlet temperature of hot fluid [K], and inlet temperature of cold fluid [K], respectively. If the absolute value of $dTF_{2,1}$ was less than 10^{-8}:

$$LMTD = dTF_1 \quad \text{(S4)}$$

If not:

$$LMTD = \frac{dTF_{2,1}}{\ln\frac{dTF_2}{dTF_1}} \quad \text{(S5)}$$

2. Calculated the heat transfer area (A) of HX tubes using **Eq. 6**.

$$A = \frac{Q}{U \cdot LMTD \cdot ft} \quad \text{(S6)}$$

where Q was the heating duty (including environmental losses) [$kJ \cdot hr^{-1}$] of the heat exchanger, U was the enforced total heat transfer efficiency [$kW \cdot m^{-2} \cdot K^{-1}$], and *ft* was the *LMTD* correction factor and can be calculated based on equations in Fahkeri et al.- If A was less than 150 ft^2, we assumed the heat exchanger type to be double pipe. If not, we assumed the heat exchanger type to be floating head.

3. Calculated the purchase cost [2013$] of the HTL heat exchanger based on the type using **Eq. 7** or **Eq. 8** and converted the cost to 2020$.

$$\text{purchase cost (double pipe)} = e^{7.2718+0.16 \cdot \ln A} \quad \text{(S7)}$$

$$\text{purchase cost (floating head)} = e^{12.0310-0.8709 \cdot \ln A+0.09005 \cdot (\ln A)^2} \quad \text{(S8)}$$

ii. Catalytic hydrothermal gasification (CHG)

HTL aqueous phase had very high COD content, therefore, cannot be discharged directly. CHG was used in our system after struvite precipitation (discussed below) to valorize COD to fuel gases. Heterogeneous catalyst 7.8% Ru/C (7.8% w/w ruthenium on a carbon support) was used in CHG.[19] About 56.55% of carbon was gasified into CH_4, C_2H_6, C_3H_8, and CO_2, with the ratio (**Table S6**) referred to by Jones et al.[19] CHG products were then passed to a flash vessel to separate gas based on vapor-liquid-equilibrium (VLE). Gas components were sent to a combined heat and power (CHP) unit and can provide energy and electricity for the system.[34] The rest of carbon and nitrogen were assumed to be in the forms of HCO_3^- and NH_4^+ in CHG effluent.[19]

Table S6. CHG, hydrotreating, and hydrocracking products (values shown in w/w).

Product	CHG[a]	hydrotreating	hydrocracking
H_2	0.0001	–	–
CO_2	0.432	–	0.0388
Methane	0.527	0.0228	0.0063
Ethane	0.011	0.0292	–
Propane	0.030	0.0165	–
Butane	–	0.0087	–
Butane, 2-methyl-	–	0.0041	–
Pentane	–	0.0068	–
Pentane, 2-methyl-	–	0.0041	–
Hexane	–	0.0041	0.0116
Hexane, 2-methyl-	–	0.0041	–
Heptane	–	0.0041	0.1202
Cyclohexane, methyl-	–	0.0102	–
Piperidine	–	0.0041	–
Toluene	–	0.0102	–
Heptane, 3-methyl-	–	0.0102	–

Octane	–	0.0102	0.0851
Cyclohexane, ethyl-	–	0.0041	–
Ethylbenzene	–	0.0204	–
o-Xylene	–	0.0102	–
Nonane	–	0.0102	0.0952
Cyclohexane, propyl-	–	0.0041	–
Benzene, propyl-	–	0.0102	–
Nonane, 4-methyl-	–	–	–
Decane	–	0.0204	0.1231
Benzene, butyl-	–	0.0122	–
Undecane	–	0.0204	0.1764
1-Phenyl-1-butene	–	0.0204	–
Dodecane	–	0.0204	0.1382
Tridecane	–	–	0.0974
Tetradecane	–	–	0.0486
Naphthalene, 1,2,3,4-tetrahydro-	–	0.0102	–
Benzene, hexyl-	–	0.0204	–
Naphthalene, 1,2,3,4-tetrahydro-6-methyl	–	0.0204	–
Benzene, heptyl-	–	0.0204	–
Benzene, octyl-	–	0.0204	–
1,4-Cyclohexanedicarboxylic acid, dimethyl ester	–	0.0184	–
Pentadecane	–	0.0612	0.0340
Hexadecane	–	0.1836	0.0201
Heptadecane	–	0.0816	0.0045
Octadecane	–	0.0408	0.0010
Nonadecane	–	0.0408	0.0052
Eicosane	–	0.1020	0.0003
Heneicosane	–	0.0408	–
Tricosane	–	0.0408	–
1,2-Benzenedicarboxylic acid, diisooctyl ester	–	0.0082	–
Heptyl undecyl phthalate	–	0.0102	–
Triacontane	–	0.0020	–

[a] Not including H_2O and soluble components.

iii. Hydrotreating

Biocrude from HTL needed to be further upgraded to meet the market requirement. Widely used hydrotreating followed by hydrocracking (next section) was selected for HTL biocrude refinement. Major assumptions made for hydrotreating were:

1. The H_2 amount reacted was assumed to be fixed at 4.6 wt% of biocrude, the same as previous work.[23] However, to maintain a H_2 headspace and ensure complete reaction, 3 times the reacted H_2 amount was fed.[19]
2. 87.5 wt% of biocrude and reacted H_2 were converted to hydrocarbon with CoMo/alumina (cobalt molybdenum on an alumina support) as the catalyst.[19]

3. The hydrotreating products were scaled from the reference. The percentages of each product can be found in **Table S6**.
4. One flash vessel and three distillation columns in series were used to separate hydrotreating products into aqueous, fuel gas, naphtha, diesel, and heavy oil. The aqueous phase was discharged and managed at a water resource recovery facility (WRRF; a.k.a. wastewater treatment plant, WWTP), fuel gases were burnt in the CHP system, naphtha and diesel were cooled down before storage, and heavy oil was further cracked in a hydrocracking unit. Flash vessel and distillation columns were inherited from BioSTEAM.

iv. Hydrocracking

Hydrocracking further broke down heavy oil from hydrotreating to naphtha and gasoline. Major assumptions for hydrocracking design included:

1. The amount of H_2 reacted was assumed to be fixed at 1.1 wt% of heavy oil, the same as previous work.[23] However, to maintain a H_2 headspace and ensure complete reaction, 5.6 times the amount of reacted H_2 was fed.[19]
2. 100 wt% of heavy oil and reacted H_2 was converted to hydrocarbon with CoMo/alumina as the catalyst.[19]
3. The hydrocracking products were scaled from the reference. The percentages of each product can be found in **Table S6**.
4. One flash vessel and one distillation column were used to separate hydrocracking products into fuel gas, naphtha, and diesel. Fuel gas was burnt in the CHP system; naphtha and diesel were cooled down before storage.

v. Phosphorus recovery

86% of phosphorus stayed in HTL produced hydrochar and could be extracted and recovered as fertilizers.[24,25] Therefore, an acid extraction followed by struvite precipitation was proposed for phosphorus recovery. According to proposed system flow, an average of 70% (49.9% to 90.2%) phosphorus[24,25] in hydrochar was extracted by acid (0.5 M H_2SO_4, 1:10 g·mL^{-1}). Then, phosphorus-rich extractant was mixed with the NH_4^+-rich HTL aqueous stream for struvite precipitation, supplemented with $MgCl_2$ (molar ratio Mg:PO_4^{3-} = 1.5:1 to 4:1) and NH_4Cl (if needed, to ensure excess amount of N). MgO was also added to maintain a pH of around 9.5.[35] The reported K_{sp} of struvite in the literature is usually smaller than 10^{-10}.[36] Therefore, instead of using a kinetic model (which always predicted ~100% phosphorus precipitation), we estimated phosphorus recovery based on published experimental data and assumed the baseline struvite precipitation recover 82.8% of phosphorus.[25]

vi. Nitrogen recovery

Part of the nitrogen in the HTL aqueous phase was recovered with phosphorus during struvite precipitation. The rest of the nitrogen (both organic and inorganic) was converted to NH_4^+ during CHG. The high concentration of NH_4^+ precluded the possibility of direct discharge of CHG effluent. A membrane distillation unit was therefore modeled to recover NH_4^+ as ammonium sulfate. The driving force of the membrane distillation was the vapor pressure difference of NH_3 across a hydrophobic membrane generated due to different temperature and pH between the feed side

and permeate side. 0.5 M H_2SO_4 was used to produce ammonium sulfate in the permeate side. The flux of ammonia across the membrane was calculated using the equation below:[37]

$$J_{NH_3,f} = k_f C_{NH_3,f} ln(\frac{X_{NH_3,f,m} - X_{NH_3,p}}{X_{NH_3,f} - X_{NH_3,p}}) \quad \text{(S9)}$$

k_f was the feed side mass transfer coefficient and can be calculated using **Eq. S10**.[38] C_{NH3} was the concentration of NH_3 in the feed and can be calculated as a function of feed pH value. $X_{NH3,f,m}$, $X_{NH3,f}$, and $X_{NH3,p}$ were NH_3 molar fractions in membrane, feed, and permeate, respectively. $X_{NH3,p}$ was approximated as 0 due to low pH in the permeate. $X_{NH3,f,m}$ and $X_{NH3,f}$ were calculated using the established VLE relationship in BioSTEAM.

$$\frac{1}{K_a} = \frac{1}{k_f} + \frac{1}{Hk_m}(1 + \frac{k_b}{[OH^-]}) \quad \text{(S10)}$$

K_a was the overall mass transfer coefficient and was estimated based on published experimental data.[38] H was dimensionless Henry's law constant and was calculated using **Eq. S11**.[39] k_m represented the membrane mass transfer coefficient and was calculated using **Eq. S12**.[38] k_b was the base dissociation constant of NH_3 and can be calculated by **Eq. S13**.

$$H = \frac{H'}{RT} \quad \text{(S11)}$$

H' is the Henry's law constant with dimension for NH_3 (1.63 $Pa \cdot m^3 \cdot mol^{-1}$). R is the ideal gas constant (8.3145 $Pa \cdot m^3 \cdot mol \cdot K^{-1}$) and T is the influent aqueous temperature (333.15 K).

$$k_m = \frac{D_m \varepsilon}{\tau \delta} \quad \text{(S12)}$$

ε, τ, and δ were membrane porosity, tortuosity, and thickness, respectively. D_m was the molecular diffusivity of ammonia in air.[40]

$$k_b = \frac{k_w}{k_a} \quad \text{(S13)}$$

k_w was the water dissociation equilibrium constant. ka was the acid dissociation constant of NH_4^+ at 333.15 K and can be adjusted based on the van't Hoff equation (**Eq. S14)**.

$$\ln\left(\frac{k_a}{k_{a,0}}\right) = \frac{\Delta H^0}{R}\left(\frac{1}{T_0} - \frac{1}{T}\right) \quad \text{(S14)}$$

$K_{a,0}$ was the acid dissociation constant of NH_4^+ at T_0 (298 K). ΔH^0 was the standard enthalpy of the NH_4^+ dissociation reaction (52.22 $kJ \cdot mol^{-1}$) at T_0.

The baseline values and distribution of other parameters included in this section can be found in **Table S11**.

vii. Unit designs

The designs (dimensions and material usage) of HTL, CHG, hydrotreating, hydrocracking, acid extraction (AcidEx), and struvite precipitation (StruPre) were done using BioSTEAM design tools. Detailed parameters can be found in **Table S7**. The flash vessel and distillation column were inherited from BioSTEAM without changes.

Table S7. Design parameters for unit operations in the HTL-based treatment train (100 dry tonne·day^{-1} capacity).

Parameter	HTL	CHG	hydrotreating	hydrocracking	AcidEx	StruPre
Temperature (T) [°C]	351	349	402	451	25	25
Pressure (P) [MPa]	21.0	21.2	10.5	7.0	0.1	0.1
# of reactors (N) [-]	4	6	1	1	2	2
Single reactor volume [m^3]	3.65	2.37	11.4	6.11	10	20
Length [m]	152	2.3	3.9	3.1	3.7	4.7
Inner diameter [m]	0.18	1.15	1.94	1.57	1.85	2.33
Wall thickness [m]	0.03	0.18	0.14	0.11	0.01	0.01
Tau[a] [h]	0.25	0.33	0.5	5	2	1
Type	pressure vessel (PV)	PV	PV	PV	storage tank	storage tank
Material	stainless steel (SS) 316	SS 316	SS 316	SS 316	SS 304	carbon steel
Vessel type	Horizontal	vertical	vertical	vertical	vertical	vertical
WHSV[b] [$g \cdot g^{-1} \cdot h^{-1}$]	–	3.56	0.625	0.625	–	–

[a] Retention time.

[b] Weight hourly space velocity.

S3. Mass and energy balance

Using QSDsan, the influent and effluent streams of each unit were automatically simulated to determine the mass and energy flows, enabling mass balances for key elements (i.e., carbon, nitrogen, and phosphorus). Energy balances considered heating/cooling of units, thermal losses, and streams' chemical energy (measured as higher heating values, HHVs). For streams consisting of defined chemicals (e.g., diesel consisting of chemicals listed in **Table S6**), we used BioSTEAM for HHV calculations. For streams that did not require full characterization or for which full composition details were unknown (e.g., organic wastes), we estimated their elemental composition and calculated their HHV using the Dulong equation:[41]

$$\text{HHV } (\text{MJ}\cdot\text{kg}^{-1}) = 0.338 \times \text{C\%} + 1.428 \times (\text{H\%} - 0.125 \times \text{O\%}) \quad \text{(S15)}$$

where C%, H%, and O% represent dry weight% of carbon, hydrogen, and oxygen, respectively.

S4. Techno-economic analysis (TEA)

The capital cost and operation and maintenance cost calculations were automated using existing algorithms in QSDsan.[42] The capital costs (purchase cost and total installed cost, TIC) for key equipment in the HTL-based system was listed in **Table S8**. Information for operation and maintenance cost estimation (e.g., chemical prices, labor costs) were included in **Table S9**.

Table S8. Capital costs for key equipment in an HTL-based system (100 dry tonne·day^{-1} capacity).

Equipment	Purchase cost [$]	Total Installed cost [$]
HTL		
Feedstock pump	92,400	159,000
Reactor heater	875,000	1,480,000
HTL reactor	1,800,000	3,540,000
Knockout drum	605,000	1,500,000
Solids filter & oil/water separator	432,000	820,000
CHG		
Feed pump	98,000	169,000
Hydrocyclone	791,000	1,660,000
Guard bed	35,400	70,800
GHG reactor	1,460,000	3,600,000
Hydrotreating & Hydrocracking		
HT reactor	414,000	1,020,000
HC reactor	271,000	667,000
CHP[a]		
CHP (total)	N/A[b]	12,400,000
CHP (allocated to HTL)	N/A	4,860,000
CHP (allocated to CHG)	N/A	5,160,000
CHP (allocated to HT & HC)	N/A	1,790,000

[a] The cost of CHP was allocated to different based on percentage of energy provided (HTL: 39.2%, CHG: 41.7%, hydrotreating & hydrocracking: 14.4%, exported as electricity: 4.8%).

[b] Only the installed cost of CHP was calculated using equations from Shoener et al.[34] and Havukainen et al.[43]

Integrated TEA-LCA were performed based on *n*th plant assumptions, which exclude any cost and environmental impacts due to technological immaturity (consistent with the standards of practice in bioenergy assessments[6,19]). We used discounted cash flow rate of return analyses to calculate the waste management cost and (separately) the minimum diesel selling price (MDSP). Specifically, the initial capital costs (CAPEX) were distributed over the plant's lifetime with a discount rate to account for the time value of money. Operation and maintenance (O&M) cost were determined by the QSDsan cost algorithms with assumptions in **Table S9**. For auxiliary units (e.g., knockout drum, sulfur guard), costs were scaled using parameters provided in Jones et al.[19] Detailed TEA procedures can be found in the QSDsan tutorial paper.[17]

Table S9. TEA baseline assumptions.

Parameters	Values
Internal rate of return	3% (waste) / 10% (biofuel)
Project lifetime	30 years
Income tax	35%
Yearly operating days	330
Construction schedule	3 years(8% 1st year, 60% 2nd year, 32% 3rd year)
Startup month	6
Startup fixed operating cost fraction	1
Startup sales fraction	0.5
Startup volatile operating cost fraction	0.75
Working capital over fixed capital investment (FCI)	5%
Finance interest	3% (waste) / 8% (biofuel)
Finance years	10
Finance fraction	0.6
Warehouse	4% of installed equipment cost
Site development	9% of inside battery limits (ISBL)
Additional piping	4.5% of ISBL
Proratable costs	10% of total direct cost (TDC)
Field expenses	10% of TDC
Home office and construction	20% of TDC
Project Contingency	10% of TDC
Other indirect costs	10% of TDC
Labor cost [$·yr^{-1}]	2.5×10^6
Labor burden	90%
Property insurance and taxes	0.7% of FCI
Maintenance	3% of total indirect cost
Steam power depreciation	MACRS20

S5. Life cycle assessment (LCA)

Unit environmental impacts of the HTL-based system were estimated based on the raw material requirements and emissions during construction and operation of the facility. We report environmental impacts across nine impact categories from the U.S. EPA's Tool for the Reduction and Assessment of Chemicals and Other Environmental Impacts (TRACI).[44] Life cycle inventory data were gathered from the Ecoinvent v3.8 database.[45] A summary of the unit impacts for raw materials, ancillary inputs, and unit processes are summarized below. The nine impact categories include global warming potential (GWP; a.k.a. carbon intensity, CI), acidification (ACD), ecotoxicity (ECO), eutrophication (EUT), ozone depletion (OZD), photochemical oxidation (PHO), carcinogenics (CAR), non-carcinogenics (NCA), and respiratory effects (RES). The values of unit impacts for each individual construction item, material, and energy source are listed in **Table S10**. A detailed description of LCA algorithms was provided in Li et al.[17]

Table S10. Unit impacts of raw materials, ancillary inputs, and unit processes.

Raw Materials, Ancillary Inputs, Unit Processes	Unit	GWP	ACD	ECO	EUT	OZD	PHO	CAR	NCA	RES
		kg CO_2-eq	$[H^+]$-eq	kg 2,4-D-eq	kg N-eq	kg CFC-11-eq	kg NO_x-eq	kg benzene-eq	kg toluene-eq	kg $PM_{2.5}$-eq
Furnace	kg	1.26	0.45675	2.5042	0.00047234	7.1820E−08	0.0036727	0.044932	49.582	0.0026779
Concrete	kg	0.11295	0.019506	0.048836	2.4132E−05	6.02E−09	0.0003157	0.00022	1.2785	0.00007732
Compressor (4kW)	ea	670.18	532.58	3736.8	0.2647	4.55E−05	2.5206	90.241	79229	2.891
Compressor (300kW)	ea	12540	8314.4	57484	4.2713	0.00077645	43.493	1361.3	1215800	47.312
Stainless steel	kg	4.8562	1.2979	7.2036	0.00083218	1.96E−07	0.012186	0.13854	164.73	0.016851
Carbon steel	kg	2.0028	0.40517	2.0272	0.00060429	8.76E−08	0.0048205	0.010698	25.211	0.0031905
Reinforcing steel	kg	2.169	0.41317	1.7266	0.00048311	1.02E−07	0.0053051	0.007312	24.747	0.0032199
RO membrane	m^2	2.2663	0.53533	0.90848	0.0028322	2.55E−07	0.0089068	0.034791	31.8	0.0028778
H_2SO_4	kg	0.008206	0.019679	0.069909	4.05E−06	8.94E−10	5.04E−05	1.74E−03	1.6824	9.41E−05
$MgCl_2$	kg	2.8779	0.77016	0.97878	0.00039767	4.94E−08	0.0072306	0.005094	8.6916	0.004385
H_2	kg	1.5624	0.81014	0.42747	0.0029415	1.80E−06	0.0052545	0.002627	8.5687	0.0036698
MgO	kg	1.1606	0.12584	2.7949	0.00063607	1.54E−08	0.0017137	0.018607	461.54	0.0008755
NaOH	kg	1.2514	0.33656	0.77272	0.00032908	7.89E−07	0.0033971	0.007004	13.228	0.0024543
NH_4Cl	kg	1.525	0.34682	0.90305	0.0047381	9.22E−08	0.0030017	0.010029	14.85	0.0018387
Struvite	kg	0.42085	0.12283	0.26961	0.00017495	2.2955E−08	0.0010441	0.002983	4.4965	0.0006176

$(NH_4)_2SO_4$	kg	1.2499	0.72917	3.4746	0.0024633	6.12E−08	0.0044519	0.036742	62.932	0.0031315
Natural gas	kg	1.5842	0.083823	0.063446	7.25E−05	1.2338E−07	0.0009737	0.000666	3.6320	0.00035092
Electricity	kWh	0.67848	0.158	0.26664	9.42E−05	2.02E−08	0.0015334	0.001125	2.1274	0.0013398
Diesel	kg	0.47694	0.25164	0.18748	0.0010547	6.42E−07	0.0019456	0.000693	2.9281	0.0011096
CHG catalyst	kg	484.76	991.65	15371	0.45019	2.2341E−05	6.7354	1.6168	27306	3.51717965
Hydrotreating & hydrocracking catalyst	kg	6.1901	4.0451	50.260	0.0057495	1.3746E−06	0.029472	0.28738	369.47	0.02072
Al_2O_3	kg	1.5976	0.59951	1.7233	0.00042279	1.50E−07	0.005035	0.011164	14.368	0.0027805
Deionized water	kg	0.000302	0.000117	0.005015	7.31E−08	1.61E−10	7.46E−07	6.19E−06	0.009977	6.89E−07
H_3PO_4	kg	1.3291	0.87049	2.5164	0.00066305	1.47E−07	0.004309	0.062976	61.475	0.0044926
MoO_3	kg	7.9395	10.629	303.18	0.0078753	3.05E−07	0.11306	0.10345	629.38	0.059407
CoO	kg	31.053	19.785	85.906	0.034405	3.78E−06	0.081471	3.1156	3167.2	0.099498
Sulfur	kg	0.12414	0.47894	0.028032	4.20E−05	1.53E−08	0.0003138	0.000152	1.2511	0.0022545
Hydrogen	kg	1.5624	0.81014	0.42747	0.0029415	1.80E−06	0.0052545	0.002627	8.5687	0.0036698
Activated carbon	kg	2.9998	0.99434	3.0363	0.00042365	8.81E−08	0.0076183	0.008292	17.436	0.0048919
Rhodium	kg	81893	168410	2612400	76.454	0.0037726	1143.7	273.49	4638900	597.08
Cl_2	kg	0.94164	0.24282	0.57521	0.0002285	5.71E−07	0.0023602	0.005184	8.4166	0.0019114
N_2	kg	0.41978	0.098525	0.1681	6.13E−05	1.09E−08	0.0009964	0.000704	1.4612	0.00084699
Cooling	MJ	0.066033	0.008253	0.025761	5.99E−06	4.89E−09	7.29E−05	0.000418	0.46216	5.06E−05
Natural gas (MJ)	MJ	0.064337	0.003404	0.002577	2.95E−06	5.01E−09	3.95E−05	2.71E−05	0.1475	1.43E−05
Steam	MJ	0.11946	0.020162	0.050719	1.58E−05	8.84E−09	0.0001616	0.000121	0.30595	9.53E−05

S6. Uncertainty analysis

The criteria for the selection of uncertainty distributions followed guidance by Li et al.[46] with modification.

Criterion 1. For parameters where the distributions can be found in literature (e.g., MCA model coefficients), we used the same distributions as the literature.

Criterion 2. For parameters where only the ranges can be found in literature (e.g., sludge moisture), we chose a uniform distribution with the minimum and maximum limits as the lower and upper bounds of the distribution and the average value of the minimum and maximum limits as the baseline.

Criterion 3. For parameters where only a single value can be found in the literature and is based on empirical formulae (e.g., elemental coefficients in **Table S2**), this value was assigned as the baseline and uniform distributions were set from 90% to 110% of the baseline value.

Criterion 4. For parameters with no known distribution in the literature:

- Criterion 4.1. If more than 20 data points were found in the literature, we selected triangular distributions and used 5^{th}, 50^{th}, and 95^{th} percentiles from the literature values as the minimum, most probable, and maximum values.
- Criterion 4.2. If only 5 to 20 data points were found in the literature, we selected triangular distributions and used minimum, average, and maximum of the literature value as the minimum, most probable, and maximum values.
- Criterion 4.3. If less than 5 data points can be found in the literature, we selected uniform distributions and used 80%, 100%, and 120% of the average value as lower bound, baseline, and upper bounds.

A complete list of distributions for each parameter used in the model can be found below (**Table S11**).

Table S11. List of parameters included in the uncertainty analyses. TP = technological parameters; DV = decision variables; CP = contextual parameters.

Parameters[a]	TP	DV	CP	Unit	Criterion	Dist.	Lower	Baseline	Upper	Std Dev
Feedstock characteristics										
ww_2_dry_sludge[b]			•	dry tonne·d^{-1}·MGD^{-1}	#3	Uniform	0.846	0.94	1.034	
sludge_moisture			•	-	#2	Uniform	0.6	0.7	0.8	
sludge_dw_ash			•	-	#4.2	Triangular	0.174	0.257	0.414	
sludge_afdw_lipid			•	-	#4.2	Triangular	0.08	0.204	0.308	
sludge_afdw_protein			•	-	#4.2	Triangular	0.38	0.463	0.51	

fog_moisture	•	-	#2	Uniform	0.1	0.35	0.6
fog_dw_ash	•	-	#4.3	Uniform	0.015	0.019	0.022
fog_afdw_lipid	•	-	#4.2	Triangular	0.912	0.987	1
fog_afdw_protein	•	-	#4.2	Triangular	0	0.002	0.012
food_moisture	•	-	#2	Uniform	0.68	0.74	0.80
food_dw_ash	•	-	#4.2	Triangular	0.025	0.0679	0.126
food_afdw_lipid	•	-	#2	Uniform	0.13	0.22	0.30
food_afdw_protein	•	-	#2	Uniform	0.15	0.2	0.25
green_moisture	•	-	#4.2	Triangular	0.052	0.342	0.69
green_dw_ash	•	-	#4.2	Triangular	0.012	0.134	0.483
green_afdw_lipid	•	-	#2	Uniform	0.0104	0.018	0.0259
green_afdw_protein	•	-	#2	Uniform	0.016	0.049	0.082
manure_moisture	•	-	#4.2	Triangular	0.174	0.663	0.798
manure_dw_ash	•	-	#4.2	Triangular	0.138	0.306	0.43
manure_afdw_lipid	•	-	#4.2	Triangular	0.038	0.092	0.247
manure_afdw_protein	•	-	#4.2	Triangular	0.143	0.216	0.264
lipid_2_C	•	-	#3	Uniform	0.675	0.75	0.825
protein_2_C	•	-	#3	Uniform	0.491	0.545	0.600
carbo_2_C	•	-	#3	Uniform	0.36	0.4	0.44
lipid_2_H	•	-	#3	Uniform	0.113	0.125	0.138
protein_2_H	•	-	#3	Uniform	0.061	0.068	0.075
carbo_2_H	•	-	#3	Uniform	0.06	0.067	0.073
protein_2_N	•	-	#3	Uniform	0.143	0.159	0.175
sludge_N_2_P	•	-	#4.2	Triangular	0.194	0.393	0.556
fog_N_2_P	•	-	#4.2	Triangular	0	0.011	0.035
food_N_2_P	•	-	#4.2	Triangular	0.115	0.150	0.286
green_N_2_P	•	-	#3	Uniform	0.187	0.208	0.229
manure_N_2_P	•	-	#4.3	Uniform	0.253	0.317	0.380
operation_hour	•	$hr \cdot yr^{-1}$	#1	Triangular	7390	7920	8450
HTL							
heating U	•	$kW \cdot m^{-2} \cdot K^{-1}$	#2	Uniform	0.0170	0.0199	0.0227

lipid_2_biocrude	•	-	#1	Triangular	0.692	0.846	1	
protein_2_biocrude	•	-	#1	Normal		0.445		0.030
carbo_2_biocrude	•	-	#1	Normal		0.205		0.050
protein_2_gas	•	-	#1	Normal		0.074		0.020
carbo_2_gas	•	-	#1	Normal		0.418		0.030
biocrude_C_slope	•	-	#1	Normal		–8.37		0.939
biocrude_C_intercept	•	-	#1	Normal		68.6		0.367
biocrude_N_slope	•	-	#1	Normal		0.133		0.005
biocrude_H_slope	•	-	#1	Normal		–2.61		0.352
biocrude_H_intercept	•	-	#1	Normal		8.20		0.138
HTLaqueous_C_slope	•	-	#1	Normal		478		18.878
TOC_TC	•	-	#1	Triangular	0.715	0.764	0.813	
hydrochar_C_slope	•	-	#1	Normal		1.750		0.122
biocrude_moisture_content	•	-	#4.2	Triangular	0.035	0.0631	0.102	
hydrochar_P_recovery_ratio	•	-	#2	Uniform	0.84	0.86	0.88	
Acid Extraction								
acid_vol	•	-	#2	Uniform	4	7	10	
P_recovery_ratio	•	-	#2	Uniform	0.7	0.8	0.9	
Struvite Precipitation								
target_pH	•	-	#2	Uniform	8.5	9	9.5	
P_pre_recovery_ratio	•	-	#4.2	Triangular	0.7	0.828	0.95	
CHG								
WHSV	•	$kg \cdot hr^{-1} \cdot kg\ catalyst^{-1}$	#4.2	Triangular	2.86	3.56	3.99	
catalyst_lifetime	•	hr	#1	Triangular	3960	7920	15800	
gas_C_to_total_C	•	-	#4.2	Triangular	0.189	0.598	0.780	
Membrane Distillation								
influent_pH	•	-	#2	Uniform	7.91	8.16	8.41	
target_pH	•	-	#2	Uniform	10	10	11.8	
relative surface area	•	-	#3	Uniform	0.00075	0.000833	0.000917	
D_m	•	$m^2 \cdot s^{-1}$	#3	Uniform	2.05E−05	2.28E−05	2.51E−05	
porosity	•	-	#3	Uniform	0.81	0.9	0.99	

thickness	•	m	#3	Uniform	6.3E−05	7.0E−05	7.7E−05
tortuosity	•	-	#3	Uniform	1.08	1.20	1.32
K_a	•	$m \cdot s^{-1}$	#3	Uniform	1.58E−05	1.75E−05	1.93E−05
capacity	•	$kg \cdot m^{-2} \cdot h^{-1}$	#3	Uniform	5.41	6.01	6.61
Hydrotreating							
WHSV	•	$kg \cdot hr^{-1} \cdot kg\ catalyst^{-1}$	#3	Uniform	0.563	0.625	0.688
catalyst_lifetime	•	hr	#1	Triangular	7920	15800	39600
hydrogen_rxned_to_biocrude	•	-	#3	Uniform	0.0414	0.0460	0.0506
PSA_efficiency	•	-	#2	Uniform	0.8	0.9	0.9
hydrogen_excess		-	#4.3	Uniform	2.4	3	3.6
hydrocarbon_ratio	•	-	#3	Uniform	0.788	0.875	0.963
Hydrocracking							
WHSV	•	$kg \cdot hr^{-1} \cdot kg\ catalyst^{-1}$	#3	Uniform	0.563	0.625	0.688
catalyst_lifetime	•	hr	#3	Uniform	35600	39600	43600
hydrogen_rxned_to_heavy_oil	•	-	#3	Uniform	0.0101	0.0113	0.0124
hydrogen_excess	•	-	#4.3	Uniform	4.44	5.56	6.67
hydrocarbon_ratio	•	-	#3	Uniform	0.9	1	1
TEA							
IRR (waste)	•	-	#1	Triangular	0%	3%	5%
IRR (biofuel)	•	-	#1	Triangular	5%	10%	15%
HTL_TIC_factor	•	-	#1	Triangular	0.6	1.0	1.4
CHG_TIC_factor	•	-	#1	Triangular	0.6	1.0	1.4
hydrotreating_TIC_factor	•	-	#1	Triangular	0.6	1.0	1.4
CHP_unit_TIC	•	$\$ \cdot kW^{-1}$	#4.3	Uniform	980	1230	1470
makeup_water	•	$\$ \cdot kg^{-1}$	#3	Uniform	0.000475	0.000528	0.000581
5%_sulfuric_acid	•	$\$ \cdot kg^{-1}$	#4.1	Triangular	0.00599	0.00658	0.0145
$MgCl_2$	•	$\$ \cdot kg^{-1}$	#4.2	Triangular	0.525	0.545	0.57
MgO	•	$\$ \cdot kg^{-1}$	#2	Uniform	0.1	0.2	0.3
H_2	•	$\$ \cdot kg^{-1}$	#3	Uniform	1.45	1.61	1.77
NH_4Cl	•	$\$ \cdot kg^{-1}$	#2	Uniform	0.12	0.13	0.14
NaOH	•	$\$ \cdot kg^{-1}$	#3	Uniform	0.473	0.526	0.578

7.8%_Ru/C	•	$\$\cdot kg^{-1}$	#1	Triangular	67.3	135	269
membrane	•	$\$\cdot kg^{-1}$	#3	Uniform	84.0	93.3	102
natural_gas	•	$\$\cdot kg^{-1}$	#4.1	Triangular	0.121	0.168	0.361
CoMo_alumina	•	$\$\cdot kg^{-1}$	#3	Uniform	34.9	38.8	42.7
$(NH_4)_2SO_4$	•	$\$\cdot kg^{-1}$	#4.2	Triangular	0.164	0.324	0.463
gasoline	•	$\$\cdot gal^{-1}$	#4.1	Triangular	2.01	2.66	4.11
		$\$\cdot kg^{-1}$			0.708	0.939	1.45
diesel	•	$\$\cdot gal^{-1}$	#4.1	Triangular	2.40	3.13	5.34
		$\$\cdot kg^{-1}$			0.746	0.972	1.66
struvite	•	$\$\cdot kg^{-1}$	#1	Triangular	0.419	0.661	1.21
electricity price	•	$\$\cdot kWh^{-1}$	#4.2	Triangular	0.0667	0.0688	0.0718
LCA							
all impact indicators for all impact items listed in **Table S10**			#3	Uniform	0.9*X	1*X	1.1*X

[a] Explanation of parameter names are available online.[18]

[b] Only for when wastewater sludge as the feedstock and water resource recovery facility (WRRF) size as the independent variable.

S7. Supplemental results

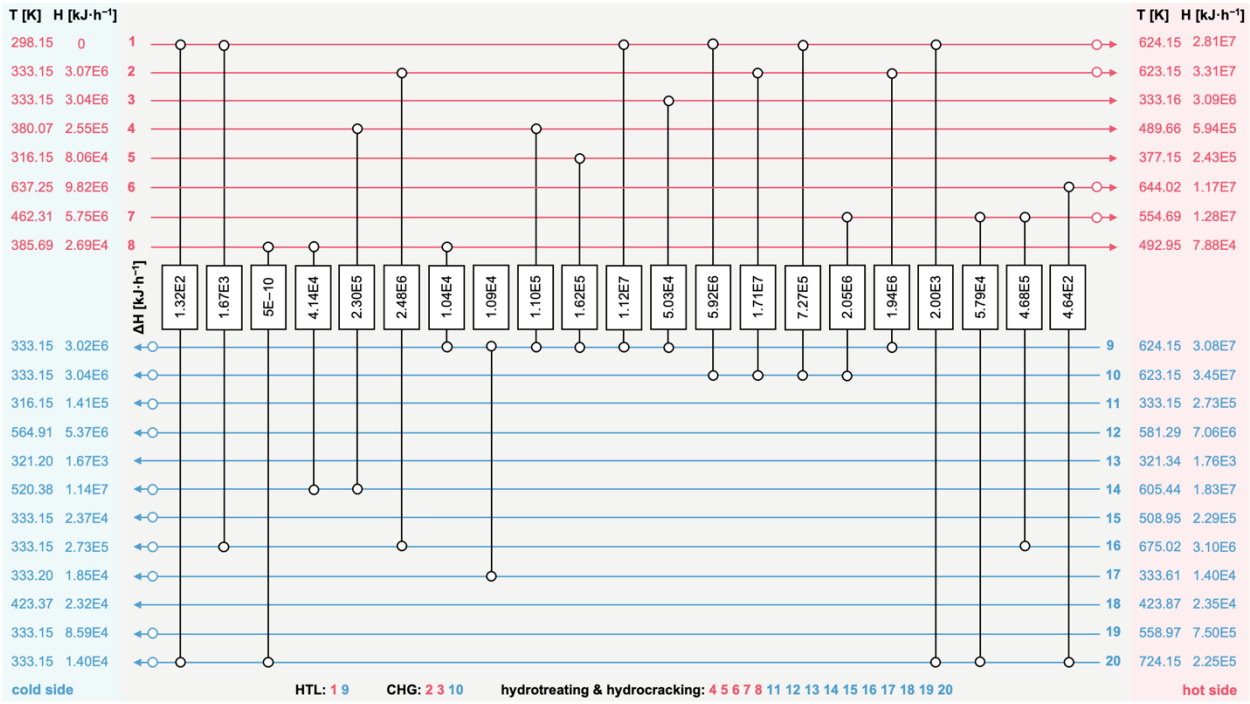

Figure S1. Pinch analysis for the heat transfers in the heat exchanger network (when the feedstock was wastewater sludge). Red horizontal lines represent streams that were heated, and blue horizontal lines represent streams that were cooled. Vertical lines bound by black outlined circles indicate heat transfer across process streams, with the amount of energy transfer marked in the middle squares. Red and blue outlined circles on horizontal lines indicate additional heating or cooling was needed for the streams to reach the final temperature. Units associated with the streams were (HTL) 1, 9; (CHG) 2, 3, 10; (hydrotreating & hydrocracking) 4, 5, 6, 7, 8, 11, 12, 13, 14, 15, 16, 17, 18, 19, 20.

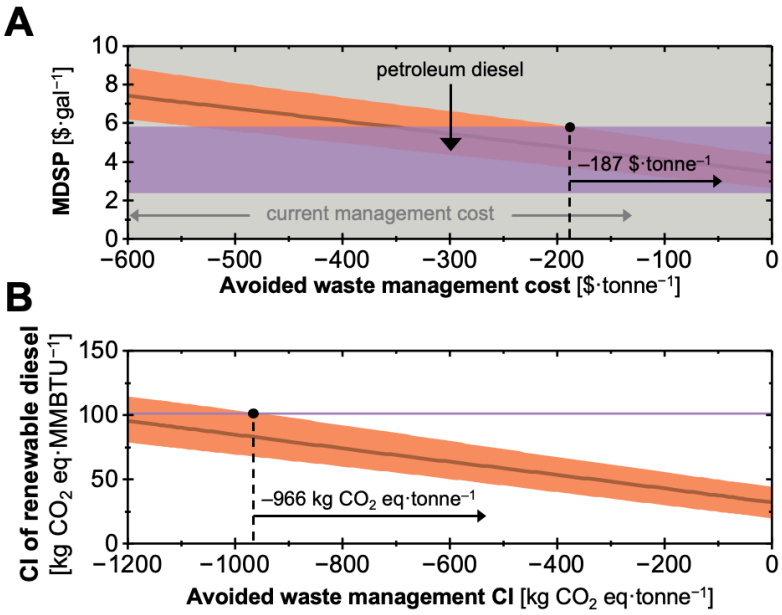

Figure S2. (A) Minimum diesel selling price (MDSP) and (B) carbon intensity (CI) of HTL-based resource recovery systems for fats, oils, and greases (FOG) as a commodity. Middle lines and the band represent 50th and 5th/95th percentiles of 1,000 Monte Carlo simulations. Purple band/line indicate the market price of diesel (data from 2018 to 2022; 2.37 to 5.81 $·gal^{-1} [47]) in (A) and petroleum diesel carbon intensity (101 kg CO_2 eq·MMBTU^{-1} [48]) in (B). Vertical dashed lines indicate the break-even point where the 95th percentile of simulated HTL-based systems is equivalent to the upper level of the current diesel price or carbon intensity. Arrows are oriented to highlight the x-axis values that represent the opportunity space for the HTL-based system.

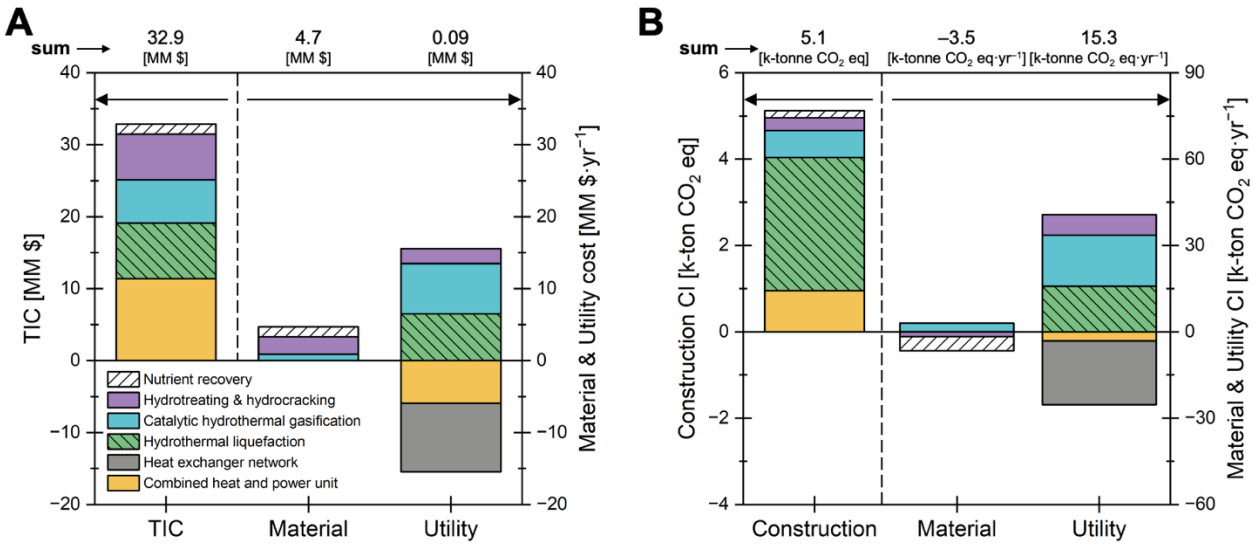

Figure S3. Breakdowns of categorized (A) cost and (B) CI to each area of the hydrothermal sludge management system. The left stacked bar in each figure is associated with the left y-axis while the middle and right stacked bars are associated with the right y-axis, as indicated by the black arrows. TIC represents the total installed cost. *Utility* in both figures includes heating, cooling, and electricity. The sum of each column is listed above the figures. A tabulated breakdown of data can be accessed online.[18]

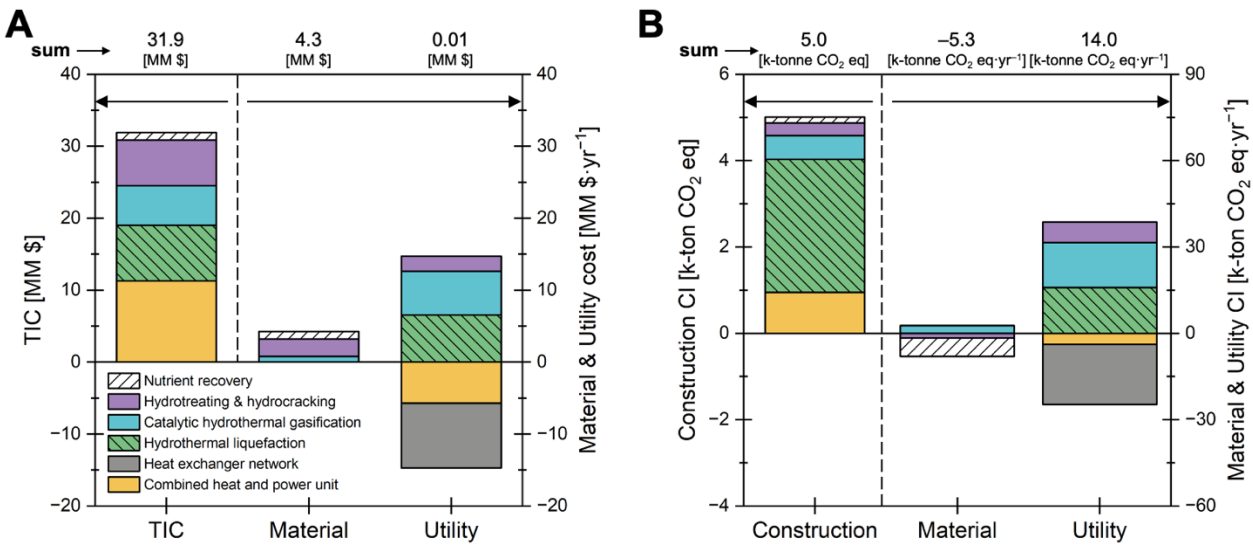

Figure S4. Breakdowns of categorized (A) cost and (B) CI to each area of the hydrothermal wastewater sludge management system (after removing the acid extraction from the original design, Alternative 1). The left stacked bar in each figure is associated with the left y-axis while the middle and right stacked bars are associated with the right y-axis, as indicated by the black arrows. TIC represents the total installed cost. *Utility* in both figures includes heating, cooling, and electricity. The sum of each column is listed above the figures. A tabulated breakdown of data can be accessed online.[18]

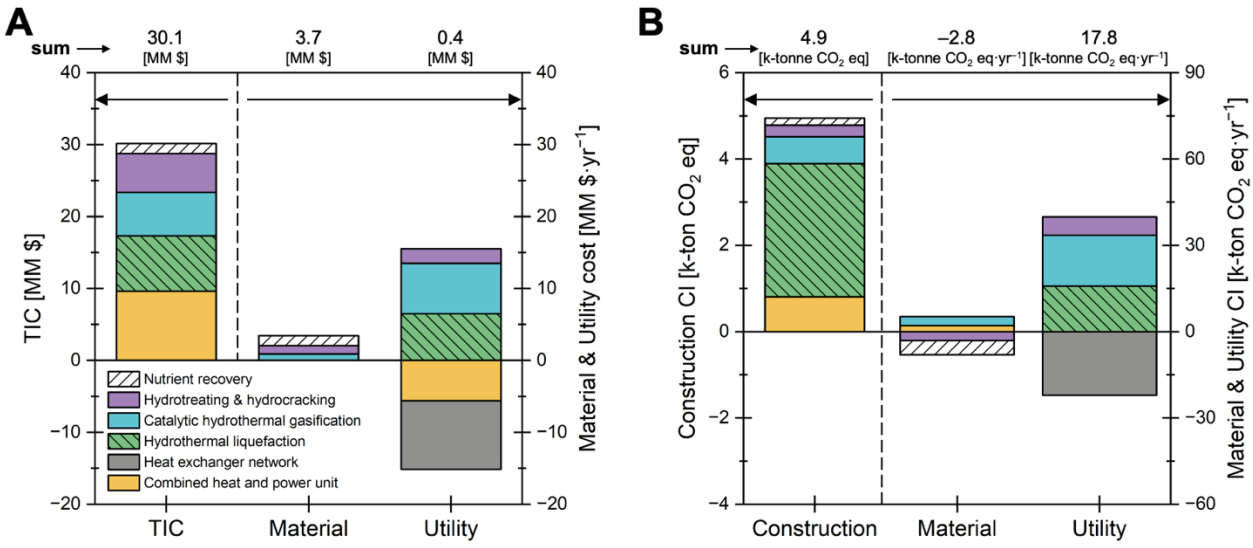

Figure S5. Breakdowns of categorized (A) cost and (B) CI to each area of the hydrothermal wastewater sludge management system (after adding a PSA unit to the original design, Alternative 2). The left stacked bar in each figure is associated with the left y-axis while the middle and right stacked bars are associated with the right y-axis, as indicated by the black arrows. TIC represents the total installed cost. *Utility* in both figures includes heating, cooling, and electricity. The sum of each column is listed above the figures. A tabulated breakdown of data can be accessed online.[18]

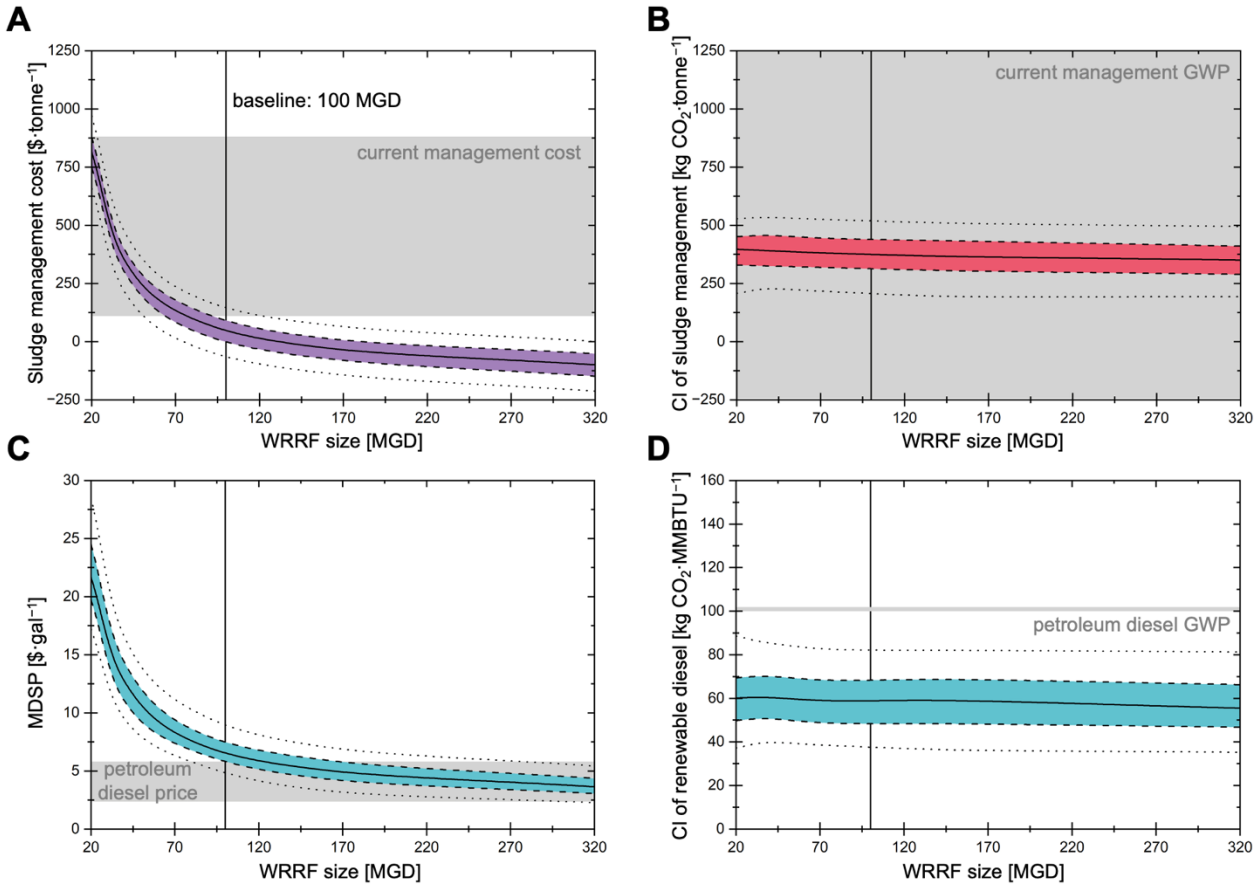

Figure S6. The effects of the water resource recovery facility (WRRF) size on (A) hydrothermal wastewater sludge management cost, (B) hydrothermal wastewater sludge management carbon intensity (CI), (C) MDSP, and (D) biofuel production CI. Figures (A) and (B) are from the waste management perspective, whereas Figures (C) and (D) are from the renewable diesel production perspective. Dotted, dashed, and the middle lines represented 5th/95th, 25th/75th, and 50th percentiles from 1,000 Monte Carlo simulations. The vertical straight lines indicate the baseline WRRF size (100 MGD) used in this study. Gray shaded areas in each figure represent (A) current wastewater sludge management cost, (B) current wastewater sludge management CI (only covers part of the current value [−245 to 2200 kg CO_2 eq·tonne^{-1}] for figure readability), (C) commercial diesel price range, and (D) petroleum diesel production CI.

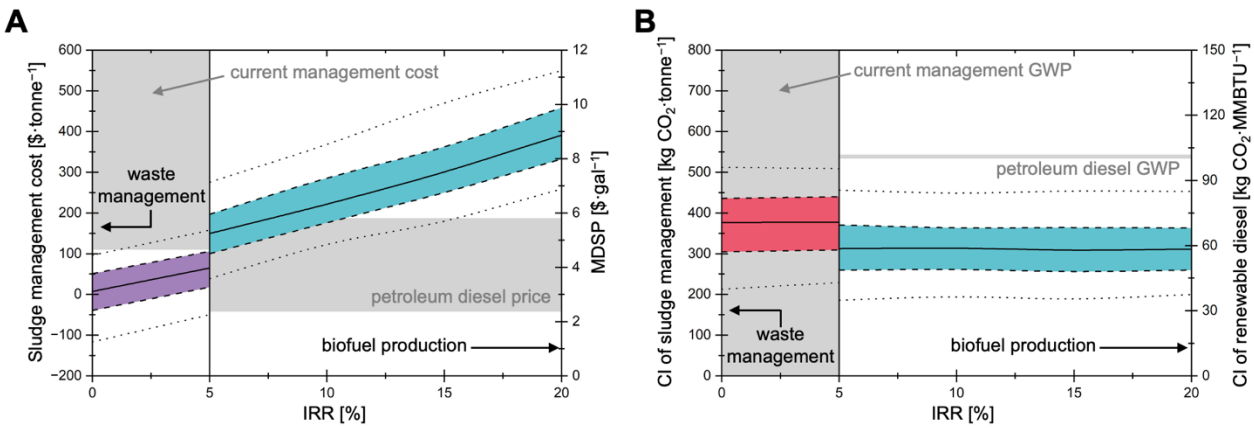

Figure S7. (A) The effects of the internal return of return on (purple, left panel) hydrothermal wastewater sludge management cost and (blue, right panel) MDSP. (B) The CI of (red, left panel) hydrothermal wastewater sludge management and (blue, right panel) biofuel production. The left side of each figure is from the waste management perspective, whereas the right side of each figure is from the renewable diesel production perspective. Dotted, dashed, and the middle lines represent 5^{th}/95^{th}, 25^{th}/75^{th}, and 50^{th} percentiles from 1,000 Monte Carlo simulations. Shaded areas in each figure represent (A, left panel) current wastewater sludge management cost (only covers part of the current value [110 to 882 $\$\cdot tonne^{-1}$] for figure readability), (A, right panel) commercial diesel price range, (B, left panel) current wastewater sludge management CI (only covers part of the current value [−245 to 2200 kg CO_2 eq·$tonne^{-1}$] for figure readability), and (B, right panel) petroleum diesel production CI.

Table S12. Element (in $kg \cdot h^{-1}$) and energy (in $GJ \cdot h^{-1}$) distribution along HTL-based treatment trains for different feedstocks.

Stream	Wastewater sludge	FOG	Food waste	Green waste	Animal manure
Carbon (C)					
Feedstock	1600	3020	1950	1350	1410
Biocrude	1030 (64%)[a]	2880 (95%)	1190 (61%)	556 (41%)	761 (54%)
Aqueous	380 (24%)	2.9 (0%)	206 (11%)	43.3 (3%)	171 (12%)
Off-gas	146 (9%)	9.9 (0%)	313 (16%)	404 (30%)	273 (19%)
Hydrochar	44.6 (3%)	2.0 (0%)	241 (12%)	351 (26%)	203 (14%)
hydrotreating naphtha	231 (14%)	589 (19%)	265 (14%)	132 (10%)	174 (12%)
hydrotreating diesel	607 (38%)	1550 (51%)	699 (36%)	348 (26%)	457 (32%)
hydrotreating heavy oil	104 (7%)	266 (9%)	120 (6%)	59.7 (4%)	78.4 (6%)
hydrotreating gas	77.8 (5%)	199 (7%)	89.5 (5%)	44.5 (3%)	58.5 (4%)
hydrotreating wastewater	10.2 (1%)	277 (9%)	19.1 (1%)	0 (0%)	0 (0%)
hydrocracking naphtha	29.9 (2%)	76.3 (3%)	34.4 (2%)	17.1 (1%)	22.5 (2%)
hydrocracking diesel	59.2 (4%)	151 (5%)	68.1 (3%)	33.9 (3%)	44.6 (3%)
hydrocracking gas	12.6 (1%)	32.2 (1%)	14.5 (1%)	7.2 (1%)	9.5 (1%)
AcidEx residual	44.6 (3%)	2.0 (0%)	241 (12%)	351 (26%)	203 (14%)
CHG influent	380 (24%)	2.9 (0%)	206 (11%)	43.3 (3%)	171 (12%)
CHG effluent	181 (11%)	1.4 (0%)	98.4 (5%)	20.7 (2%)	81.9 (6%)
CHG gas	200 (11%)	1.5 (0%)	107 (6%)	22.5 (2%)	89.5 (6%)
MemDis wastewater	181 (11%)	1.4 (0%)	98.4 (5%)	20.7 (2%)	81.9 (6%)
Nitrogen (N)					
Feedstock	214	3.0	123	25.7	98.6
Biocrude	61.1 (28%)	2.2 (72%)	40.3 (33%)	4.2 (17%)	21.1 (21%)
Aqueous	153 (72%)	0.8 (28%)	83.2 (67%)	21.5 (83%)	77.5 (79%)
hydrotreating naphtha	0.8 (0%)	2.1 (69%)	0.9 (1%)	0.5 (2%)	0.6 (1%)
hydrotreating wastewater	60.2 (28%)	0.1 (3%)	39.4 (32%)	3.8 (15%)	20.5 (21%)
Struvite	25.3 (12%)	0 (0%)	7.0 (6%)	1.7 (6%)	9.7 (10%)
CHG influent	128 (60%)	0.8 (27%)	76.2 (62%)	19.8 (77%)	67.8 (69%)
CHG effluent	128 (60%)	0.8 (27%)	76.2 (62%)	19.8 (77%)	67.8 (69%)
$(NH_4)_2SO_4$	127 (59%)	0.8 (27%)	75.8 (61%)	19.7 (77%)	67.5 (68%)
MemDis wastewater	0.6 (0%)	0 (0%)	0.3 (0%)	0.1 (0%)	0.3 (0%)
Phosphorus (P)					
Feedstock	82.0	0	22.5	5.3	31.2
Aqueous	11.5 (14%)	0 (14%)	3.2 (14%)	0.7 (14%)	4.4 (14%)
Hydrochar	70.6 (86%)	0 (86%)	19.3 (86%)	4.6 (86%)	26.9 (86%)
AcidEx extractant	56.4 (69%)	0 (69%)	15.5 (69%)	3.7 (69%)	21.5 (69%)
AcidEx residual	14.2 (17%)	0 (17%)	3.8 (17%)	0.9 (17%)	5.3 (17%)
Struvite	56.0 (68%)	0 (68%)	15.4 (69%)	3.7 (69%)	21.4 (68%)
CHG influent	11.8 (14%)	0 (15%)	3.2 (14%)	0.8 (14%)	4.5 (14%)
CHG effluent	11.8 (14%)	0 (15%)	3.2 (14%)	0.8 (14%)	4.5 (14%)

MemDis wastewater	11.8 (14%)	0 (15%)	3.2 (14%)	0.8 (14%)	4.5 (14%)
Energy (E)					
Feedstock	71.0	164	83.4	47.6	56.9
Biocrude	46.4 (65%)	152 (93%)	54.1 (65%)	23.4 (49%)	33.6 (59%)
Off-gas	2.4 (3%)	0.2 (0%)	4.5 (5%)	5.7 (12%)	3.9 (7%)
CHG gas	11.5 (16%)	0.1 (0%)	6.2 (7%)	1.3 (3%)	5.1 (9%)
hydrotreating H_2	25.9	66.1	29.5	14.8	19.4
hydrotreating naphtha	12.4 (13%)[b]	31.8 (14%)	14.3 (13%)	7.1 (11%)	9.4 (12%)
hydrotreating diesel	32.8 (34%)	83.8 (36%)	37.7 (33%)	18.8 (30%)	24.7 (32%)
hydrotreating heavy oil	5.6 (6%)	14.4 (6%)	6.5 (6%)	3.2 (5%)	4.2 (6%)
hydrotreating gas	22.4 (23%)	57.2 (25%)	25.5 (23%)	12.8 (20%)	16.7 (22%)
hydrocracking H_2	1.1	2.8	1.3	0.6	0.8
hydrocracking naphtha	1.7 (2%)[c]	4.3 (2%)	2.0 (2%)	1.0 (2%)	1.3 (2%)
hydrocracking diesel	3.3 (3%)	8.5 (4%)	3.8 (3%)	1.9 (3%)	2.5 (3%)
hydrocracking gas	1.6 (2%)	4.0 (2%)	1.8 (2%)	0.9 (1%)	1.2 (2%)

[a] % of C, N, P, or E from the feedstock.

[b] % of E from the feedstock and hydrotreating H_2.

[c] % of E from the feedstock, hydrotreating H_2, and hydrocracking H_2.

Table S13. Spearman's rank order correlation coefficients for hydrothermal wastewater sludge management (only parameters with $p < 0.05$ and $|\rho| > 0.1$ are listed). Indicators include sludge management cost, minimum diesel selling price (MDSP), the carbon intensity of sludge management from the waste management perspective (CI_{sludge}), and the carbon intensity of diesel production from the renewable diesel production perspective (CI_{diesel}).

Sub-category	Parameters	Sludge management cost	MDSP	CI_{sludge}	CI_{diesel}
Contextual parameters					
-	plant size	–0.30	–0.29	–0.06	–0.06
	internal rate of return (IRR)	0.33	0.30	–0.06	–0.07
feedstock characterization	feedstock ash content	0.34	0.47	0.43	0.56
	feedstock lipid content	–0.22	–0.37	–0.11	–0.30
	feedstock protein content	–0.12	–0.15	–0.12	–0.14
	feedstock protein:N ratio	–0.13	–0.11	–0.09	–0.06
	feedstock N:P ratio	–0.10	–0.06	0.28	0.24
material & product price	struvite price	–0.28	–0.29	–0.06	–0.05
	ammonium sulfate price	–0.12	–0.12	0.02	0.00
	gasoline price	–0.16	–0.16	–0.03	–0.02
	diesel price	–0.52	–0.02	–0.02	–0.05
Technological parameters					
HTL	lipid to biocrude conversion	–0.18	–0.25	–0.05	–0.16
	protein to biocrude conversion	–0.13	–0.21	–0.09	–0.19
	carbohydrate to biocrude conversion	–0.16	–0.24	–0.16	–0.28
	aqueous TOC:TC ratio[a]	0.01	0.01	0.14	0.11
CHG	CHG yield	0.04	–0.01	–0.43	–0.35

	catalyst lifetime	–0.05	–0.03	–0.28	–0.20
nutrient recovery	phosphorus acid extraction ratio	–0.01	–0.03	0.13	0.12
hydrotreating	reacted hydrogen amount	0.01	0.04	–0.16	–0.10
	excess hydrogen amount	0.01	0.04	–0.36	–0.27
	hydrotreating yield	–0.25	–0.32	–0.06	–0.23
Decision parameters					
-	operation hour	–0.06	–0.08	0.18	0.14

[a] Total organic carbon to total carbon ratio in the HTL aqueous phase.

Table S14. Life cycle environmental impact results across feedstocks and categories.

Feedstock	CFs	ACD	ECO	EUT	OZD	PHO	CAR	NCA	RES
	unit	$[H^+]$-eq	kg 2,4-D-eq	kg N-eq	kg CFC-11-eq	kg NO_x-eq	kg benzene-eq	kg toluene-eq	kg $PM_{2.5}$-eq
Wastewater sludge	***normalized by per tonne waste managed***								
	5th	77.8	1630	−5.46E−01	−1.11E−04	3.62E−01	1.61	5790	3.52E−01
	median	157	2610	−4.13E−01	−6.45E−05	9.38E−01	3.38	10600	7.14E−01
	95th	274	4470	−2.81E−01	−1.75E−05	1.80E+00	5.06	16600	1.24E+00
	normalized by per MMBTU diesel produced[a]								
	5th	14.9	196	−3.78E−02	4.77E−06	8.59E−02	1.67E−01	804	6.39E−02
	median	26.2	330	−2.41E−02	8.52E−06	1.67E−01	4.42E−01	1390	1.19E−01
	95th	42.8	574	−8.91E−03	1.39E−05	2.85E−01	6.96E−01	2300	1.93E−01
FOG	***normalized by per tonne waste managed***								
	5th	23.2	1580	−4.56E−01	−2.93E−04	−1.45E−01	3.81	6490	−1.74E−01
	median	104	2390	−3.01E−01	−1.97E−04	5.13E−01	4.35	8340	3.28E−01
	95th	234	3790	−1.34E−01	−9.75E−05	1.35E+00	5.00	11600	8.92E−01
	normalized by per MMBTU diesel produced[a]								
	5th	7.07	79.3	6.85E−03	3.88E−06	3.88E−02	1.95E−01	372	1.61E−02
	median	11.8	121	1.25E−02	7.12E−06	7.69E−02	2.28E−01	480	4.50E−02
	95th	17.7	199	2.02E−02	1.13E−05	1.19E−01	2.66E−01	645	7.26E−02
Food waste	***normalized by per tonne waste managed***								
	5th	140	2080	−3.67E−01	−1.27E−04	7.73E−01	4.44	15500	6.29E−01
	median	231	3220	−2.40E−01	−6.86E−05	1.44E+00	6.20	23700	1.07E+00
	95th	389	5360	−1.04E−01	−1.08E−05	2.44E+00	8.31	33100	1.63E+00
	normalized by per MMBTU diesel produced[a]								
	5th	20.6	214	−9.73E−03	4.80E−06	1.27E−01	4.53E−01	1640	8.96E−02
	median	32.3	364	2.18E−03	9.15E−06	2.12E−01	6.92E−01	2660	1.48E−01
	95th	53.3	630	1.42E−02	1.47E−05	3.48E−01	9.95E−01	4030	2.31E−01
Green waste	***normalized by per tonne waste managed***								
	5th	241	2570	−4.69E−02	−5.28E−05	1.61	5.98	23100	1.12
	median	324	3870	5.02E−02	−4.47E−05	2.18	8.06	33700	1.47
	95th	490	6460	1.63E−01	4.80E−05	3.26	10.2	45200	2.04

	normalized by per MMBTU diesel produced[a]								
	5th	47.4	491	1.70E−02	7.93E−06	3.29E−01	1.08	4550	2.21E−01
	median	78.9	851	3.91E−02	1.60E−05	5.49E−01	1.78	7380	3.58E−01
	95th	151	1800	8.09E−02	3.52E−05	1.04E+00	2.99	13000	6.64E−01
	normalized by per tonne waste managed								
	5th	167	2120	−2.65E−01	−7.73E−05	1.08E+00	3.96	15100	8.34E−01
	median	247	3250	−1.53E−01	−2.94E−05	1.65E+00	5.58	21500	1.16E+00
Animal manure	95th	381	5240	−3.79E−02	1.84E−05	2.59E+00	7.55	30700	1.66E+00
	normalized by per MMBTU diesel produced[a]								
	5th	30.6	327	−1.26E−02	6.18E−06	2.06E−01	6.20E−01	2240	1.48E−01
	median	49.8	559	2.88E−03	1.17E−05	3.30E−01	9.69E−01	3730	2.29E−01
	95th	79.1	972	1.93E−02	1.98E−05	5.34E−01	1.39E+00	5950	3.45E−01

[a] The normalization for diesel produced did not account for environmental impacts offset by avoiding traditional waste management methods.

References

(1) Grady, C. P. L., Jr.; Daigger, G. T.; Love, N. G.; Filipe, C. D. M. *Biological Wastewater Treatment*, 3rd ed.; CRC Press: Boca Raton, 2011. https://doi.org/10.1201/b13775.

(2) Lin, N.; Zhu, W.; Fan, X.; Wang, C.; Chen, C.; Zhang, H.; Chen, L.; Wu, S.; Cui, Y. Key Factor on Improving Secondary Advanced Dewatering Performance of Municipal Dewatered Sludge: Selective Oxidative Decomposition of Polysaccharides. *Chemosphere* **2020**, *249*, 126108. https://doi.org/10.1016/j.chemosphere.2020.126108.

(3) Snowden-Swan, L. J.; Billing, J. M.; Thorson, M. R.; Schmidt, A. J.; Santosa, D. M.; Jones, S. B.; Hallen, R. T. *Wet Waste Hydrothermal Liquefaction and Biocrude Upgrading to Hydrocarbon Fuels: 2019 State of Technology*; PNNL-29882; Pacific Northwest National Lab. (PNNL), Richland, WA (United States), 2020. https://doi.org/10.2172/1617028.

(4) Snowden-Swan, L. J.; Billing, J. M.; Thorson, M. R.; Schmidt, A. J.; Jiang, Y.; Santosa, D. M.; Seiple, T. E.; Daniel, R. C.; Burns, C. A.; Li, S.; Hart, T. R.; Fox, S. P.; Olarte, M. V.; Kallupalayam Ramasamy, K.; Anderson, D. B.; Hallen, R. T.; Radovcich, S.; Mathias, P. M.; Taylor, M. A. *Wet Waste Hydrothermal Liquefaction and Biocrude Upgrading to Hydrocarbon Fuels: 2020 State of Technology*; PNNL-30982; Pacific Northwest National Lab. (PNNL), Richland, WA (United States), 2021. https://doi.org/10.2172/1771363.

(5) Snowden-Swan, L. J.; Li, S.; Jiang, Y.; Thorson, M. R.; Schmidt, A. J.; Seiple, T. E.; Billing, J. M.; Santosa, D. M.; Hart, T. R.; Fox, S. P.; Cronin, D.; Kallupalayam Ramasamy, K.; Anderson, D. B.; Hallen, R. T.; Fonoll-Almansa, X.; Norton, J. *Wet Waste Hydrothermal Liquefaction and Biocrude Upgrading to Hydrocarbon Fuels: 2021 State of Technology*; PNNL-32731; Pacific Northwest National Lab. (PNNL), Richland, WA (United States), 2022. https://doi.org/10.2172/1863608.

(6) Snowden-Swan, L. J.; Li, S.; Thorson, M. R.; Schmidt, A. J.; Cronin, D. J.; Zhu, Y.; Hart, T. R.; Santosa, D. M.; Fox, S. P.; Lemmon, T. L.; Swita, M. S. *Wet Waste Hydrothermal Liquefaction and Biocrude Upgrading to Hydrocarbon Fuels: 2022 State of Technology*; PNNL-33622; Pacific Northwest National Lab. (PNNL), Richland, WA (United States), 2022. https://doi.org/10.2172/1897670.

(7) Keener, K. M.; Ducoste, J. J.; Holt, L. M. Properties Influencing Fat, Oil, and Grease Deposit Formation. *Water Environ. Res.* **2008**, *80* (12), 2241–2246. https://doi.org/10.2175/193864708X267441.

(8) da Silva Almeida, H.; Corrêa, O. A.; Eid, J. G.; Ribeiro, H. J.; de Castro, D. A. R.; Pereira, M. S.; Pereira, L. M.; de Andrade Aâncio, A.; Santos, M. C.; da Mota, S. A. P.; da Silva Souza, J. A.; Borges, L. E. P.; Mendonça, N. M.; Machado, N. T. Performance of Thermochemical Conversion of Fat, Oils, and Grease into Kerosene-like Hydrocarbons in Different Production Scales. *J. Anal. Appl. Pyrolysis* **2016**, *120*, 126–143. https://doi.org/10.1016/j.jaap.2016.04.017.

(9) Cabrera, D. V.; Labatut, R. A. Outlook and Challenges for Recovering Energy and Water from Complex Organic Waste Using Hydrothermal Liquefaction. *Sustain. Energy Fuels* **2021**, *5* (8), 2201–2227. https://doi.org/10.1039/D0SE01857K.

(10) Slopiecka, K.; Liberti, F.; Massoli, S.; Bartocci, P.; Fantozzi, F. Chemical and Physical Characterization of Food Waste to Improve Its Use in Anaerobic Digestion Plants. *Energy Nexus* **2022**, *5*, 100049. https://doi.org/10.1016/j.nexus.2022.100049.

(11) Zhang, R.; El-Mashad, H. M.; Hartman, K.; Wang, F.; Liu, G.; Choate, C.; Gamble, P. Characterization of Food Waste as Feedstock for Anaerobic Digestion. *Bioresour. Technol.* **2007**, *98* (4), 929–935. https://doi.org/10.1016/j.biortech.2006.02.039.
(12) Pour, F. H.; Makkawi, Y. T. A Review of Post-Consumption Food Waste Management and Its Potentials for Biofuel Production. *Energy Rep.* **2021**, *7*, 7759–7784. https://doi.org/10.1016/j.egyr.2021.10.119.
(13) Liu, X.; Xie, Y.; Sheng, H. Green Waste Characteristics and Sustainable Recycling Options. *Resour. Environ. Sustain.* **2023**, *11*, 100098. https://doi.org/10.1016/j.resenv.2022.100098.
(14) Komilis, D. P.; Ham, R. K. The Effect of Lignin and Sugars to the Aerobic Decomposition of Solid Wastes. *Waste Manag.* **2003**, *23* (5), 419–423. https://doi.org/10.1016/S0956-053X(03)00062-X.
(15) Nynäs, A.-L.; Newson, W. R.; Johansson, E. Protein Fractionation of Green Leaves as an Underutilized Food Source—Protein Yield and the Effect of Process Parameters. *Foods* **2021**, *10* (11), 2533. https://doi.org/10.3390/foods10112533.
(16) Lu, J.; Li, H.; Zhang, Y.; Liu, Z. Nitrogen Migration and Transformation during Hydrothermal Liquefaction of Livestock Manures. *ACS Sustain. Chem. Eng.* **2018**, *6* (10), 13570–13578. https://doi.org/10.1021/acssuschemeng.8b03810.
(17) Li, Y.; Zhang, X.; Morgan, V. L.; Lohman, H. A. C.; Rowles, L. S.; Mittal, S.; Kogler, A.; Cusick, R. D.; Tarpeh, W. A.; Guest, J. S. QSDsan: An Integrated Platform for Quantitative Sustainable Design of Sanitation and Resource Recovery Systems. *Environ. Sci. Water Res. Technol.* **2022**, 10.1039.D2EW00455K. https://doi.org/10.1039/D2EW00455K.
(18) *GitHub - QSD-Group/EXPOsan at 2c9e246bb19cb67b8f8ac52ec4b978b2b118d12a*. https://github.com/QSD-Group/EXPOsan/tree/2c9e246bb19cb67b8f8ac52ec4b978b2b118d12a (accessed 2023-11-06).
(19) Jones, S. B.; Zhu, Y.; Anderson, D. B.; Hallen, R. T.; Elliott, D. C.; Schmidt, A. J.; Albrecht, K. O.; Hart, T. R.; Butcher, M. G.; Drennan, C.; Snowden-Swan, L. J.; Davis, R.; Kinchin, C. *Process Design and Economics for the Conversion of Algal Biomass to Hydrocarbons: Whole Algae Hydrothermal Liquefaction and Upgrading*; PNNL--23227, 1126336; 2014; p PNNL--23227, 1126336. https://doi.org/10.2172/1126336.
(20) Cortes-Peña, Y.; Kumar, D.; Singh, V.; Guest, J. S. BioSTEAM: A Fast and Flexible Platform for the Design, Simulation, and Techno-Economic Analysis of Biorefineries under Uncertainty. *ACS Sustain. Chem. Eng.* **2020**, *8* (8), 3302–3310. https://doi.org/10.1021/acssuschemeng.9b07040.
(21) *GitHub - BioSTEAMDevelopmentGroup/biosteam at 0da3da0165078bbafea15caef70b17cfa40616e6*. GitHub. https://github.com/BioSTEAMDevelopmentGroup/biosteam (accessed 2023-11-06).
(22) Li, Y.; Leow, S.; Fedders, A. C.; Sharma, B. K.; Guest, J. S.; Strathmann, T. J. Quantitative Multiphase Model for Hydrothermal Liquefaction of Algal Biomass. *Green Chem.* **2017**, *19* (4), 1163–1174. https://doi.org/10.1039/C6GC03294J.
(23) Leow, S.; Shoener, B. D.; Li, Y.; DeBellis, J. L.; Markham, J.; Davis, R.; Laurens, L. M. L.; Pienkos, P. T.; Cook, S. M.; Strathmann, T. J.; Guest, J. S. A Unified Modeling Framework to Advance Biofuel Production from Microalgae. *Environ. Sci. Technol.* **2018**, *52* (22), 13591–13599. https://doi.org/10.1021/acs.est.8b03663.

(24) Matayeva, A.; Rasmussen, S. R.; Biller, P. Distribution of Nutrients and Phosphorus Recovery in Hydrothermal Liquefaction of Waste Streams. *Biomass Bioenergy* **2022**, *156*, 106323. https://doi.org/10.1016/j.biombioe.2021.106323.
(25) Ovsyannikova, E.; Kruse, A.; Becker, G. C. Feedstock-Dependent Phosphate Recovery in a Pilot-Scale Hydrothermal Liquefaction Bio-Crude Production. *Energies* **2020**, *13* (2), 379. https://doi.org/10.3390/en13020379.
(26) Motavaf, B.; Savage, P. E. Effect of Process Variables on Food Waste Valorization via Hydrothermal Liquefaction. *ACS EST Eng.* **2021**, *1* (3), 363–374. https://doi.org/10.1021/acsestengg.0c00115.
(27) Maag, A. R.; Paulsen, A. D.; Amundsen, T. J.; Yelvington, P. E.; Tompsett, G. A.; Timko, M. T. Catalytic Hydrothermal Liquefaction of Food Waste Using CeZrOx. *Energies* **2018**, *11* (3), 564. https://doi.org/10.3390/en11030564.
(28) Aierzhati, A.; Stablein, M. J.; Wu, N. E.; Kuo, C.-T.; Si, B.; Kang, X.; Zhang, Y. Experimental and Model Enhancement of Food Waste Hydrothermal Liquefaction with Combined Effects of Biochemical Composition and Reaction Conditions. *Bioresour. Technol.* **2019**, *284*, 139–147. https://doi.org/10.1016/j.biortech.2019.03.076.
(29) Ahmed Ebrahim, S.; Robertson, G.; Jiang, X.; Baranova, E. A.; Singh, D. Catalytic Hydrothermal Liquefaction of Food Waste: Influence of Catalysts on Bio-Crude Yield, Asphaltenes, and Pentane Soluble Fractions. *Fuel* **2022**, *324*, 124452. https://doi.org/10.1016/j.fuel.2022.124452.
(30) Ellersdorfer, M. Hydrothermal Co-Liquefaction of Chlorella Vulgaris with Food Processing Residues, Green Waste and Sewage Sludge. *Biomass Bioenergy* **2020**, *142*, 105796. https://doi.org/10.1016/j.biombioe.2020.105796.
(31) Cao, L.; Luo, G.; Zhang, S.; Chen, J. Bio-Oil Production from Eight Selected Green Landscaping Wastes through Hydrothermal Liquefaction. *RSC Adv.* **2016**, *6* (18), 15260–15270. https://doi.org/10.1039/C5RA24760H.
(32) Knorr, D.; Lukas, J.; Schoen, P. *Production of Advanced Biofuels via Liquefaction - Hydrothermal Liquefaction Reactor Design: April 5, 2013*; NREL/SR-5100-60462, 1111191; 2013; p NREL/SR-5100-60462, 1111191. https://doi.org/10.2172/1111191.
(33) Fakheri, A. A General Expression for the Determination of the Log Mean Temperature Correction Factor for Shell and Tube Heat Exchangers. *J. Heat Transf.* **2003**, *125* (3), 527–530. https://doi.org/10.1115/1.1571078.
(34) Shoener, B. D.; Zhong, C.; Greiner, A. D.; Khunjar, W. O.; Hong, P.-Y.; Guest, J. S. Design of Anaerobic Membrane Bioreactors for the Valorization of Dilute Organic Carbon Waste Streams. *Energy Environ. Sci.* **2016**, *9* (3), 1102–1112. https://doi.org/10.1039/C5EE03715H.
(35) Lorick, D.; Macura, B.; Ahlström, M.; Grimvall, A.; Harder, R. Effectiveness of Struvite Precipitation and Ammonia Stripping for Recovery of Phosphorus and Nitrogen from Anaerobic Digestate: A Systematic Review. *Environ. Evid.* **2020**, *9* (1), 27. https://doi.org/10.1186/s13750-020-00211-x.
(36) Hanhoun, M.; Montastruc, L.; Azzaro-Pantel, C.; Biscans, B.; Frèche, M.; Pibouleau, L. Temperature Impact Assessment on Struvite Solubility Product: A Thermodynamic Modeling Approach. *Chem. Eng. J.* **2011**, *167* (1), 50–58. https://doi.org/10.1016/j.cej.2010.12.001.

(37) Scheepers, D. M.; Tahir, A. J.; Brunner, C.; Guillen-Burrieza, E. Vacuum Membrane Distillation Multi-Component Numerical Model for Ammonia Recovery from Liquid Streams. *J. Membr. Sci.* **2020**, *614*, 118399. https://doi.org/10.1016/j.memsci.2020.118399.
(38) Ding, Z.; Liu, L.; Li, Z.; Ma, R.; Yang, Z. Experimental Study of Ammonia Removal from Water by Membrane Distillation (MD): The Comparison of Three Configurations. *J. Membr. Sci.* **2006**, *286* (1), 93–103. https://doi.org/10.1016/j.memsci.2006.09.015.
(39) Katyal, A.; Morrison, R. D. CHAPTER 11 - FORENSIC APPLICATIONS OF CONTAMINANT TRANSPORT MODELS IN THE SUBSURFACE. In *Introduction to Environmental Forensics (Second Edition)*; Murphy, B. L., Morrison, R. D., Eds.; Academic Press: Burlington, 2007; pp 513–575. https://doi.org/10.1016/B978-012369522-2/50012-9.
(40) Spiller, L. L. Determination of Ammonia/Air Diffusion Coefficient Using Nafion Lined Tube. *Anal. Lett.* **1989**, *22* (11–12), 2561–2573. https://doi.org/10.1080/00032718908052375.
(41) Brown, T. M.; Duan, P.; Savage, P. E. Hydrothermal Liquefaction and Gasification of Nannochloropsis Sp. *Energy Fuels* **2010**, *24* (6), 3639–3646. https://doi.org/10.1021/ef100203u.
(42) Li, Y.; Zhang, X.; Morgan, V. L.; Lohman, H. A. C.; Rowles, L. S.; Mittal, S.; Kogler, A.; Cusick, R. D.; Tarpeh, W. A.; Guest, J. S. QSDsan: An Integrated Platform for Quantitative Sustainable Design of Sanitation and Resource Recovery Systems. *Environ. Sci. Water Res. Technol.* **2022**, *8* (10), 2289–2303. https://doi.org/10.1039/D2EW00455K.
(43) Havukainen, J.; Nguyen, M. T.; Väisänen, S.; Horttanainen, M. Life Cycle Assessment of Small-Scale Combined Heat and Power Plant: Environmental Impacts of Different Forest Biofuels and Replacing District Heat Produced from Natural Gas. *J. Clean. Prod.* **2018**, *172*, 837–846. https://doi.org/10.1016/j.jclepro.2017.10.241.
(44) Bare, J. TRACI 2.0: The Tool for the Reduction and Assessment of Chemical and Other Environmental Impacts 2.0. *Clean Technol. Environ. Policy* **2011**, *13* (5), 687–696. https://doi.org/10.1007/s10098-010-0338-9.
(45) Ecoinvent 3.8 Database. Swiss Centre for Life Cycle Inventories (accessed 2023-01-06).
(46) Li, Y.; Bhagwat, S. S.; Cortés-Peña, Y. R.; Ki, D.; Rao, C. V.; Jin, Y.-S.; Guest, J. S. Sustainable Lactic Acid Production from Lignocellulosic Biomass. *ACS Sustain. Chem. Eng.* **2021**, *9* (3), 1341–1351. https://doi.org/10.1021/acssuschemeng.0c08055.
(47) *Gasoline and Diesel Fuel Update*. https://www.eia.gov/petroleum/gasdiesel/index.php (accessed 2023-03-14).
(48) Pegallapati, A. K.; Dunn, J. B.; Frank, E. D.; Jones, S.; Zhu, Y.; Snowden-Swan, L.; Davis, R.; Kinchin, C. M. *Supply Chain Sustainability Analysis of Whole Algae Hydrothermal Liquefaction and Upgrading*; ANL/ESD--15/8, 1183770; 2015; p ANL/ESD--15/8, 1183770. https://doi.org/10.2172/1183770.